Proceedings of the ASME 2010 3rd Joint US-European Fluids Engineering Summer Meeting and 8th International Conference on Nanochannels, Microchannels, and Minichannels
FEDSM-ICNMM2010
August 1-5, 2010, Montreal, Canada

FEDSM-ICNMM2010-30354

NEAR-WALL RANS MODELLING IN LES OF HEAT TRANSFER IN BACKWARD-FACING STEP FLOWS UNDER CONDITIONS OF CONSTANT AND VARIABLE FLUID PROPERTIES

S. Jakirlić*
Chair of Fluid Mechanics and Aerodynamics[1] and
Center of Smart Interfaces - CSI[2]
Department of Mechanical Engineering
Technische Universität Darmstadt
Petersenstr. 30[1]/32[2], D-64287 Darmstadt, Germany
s.jakirlic@sla.tu-darmstadt.de

B. Kniesner
Astrium Space Transportation
TP24 System Analysis
D-81663 Munich, Germany
bjoern.kniesner@astrium.eads.net

ABSTRACT

Two backward-facing step (BFS) flow configurations associated with the heat transfer under the conditions of constant and variable fluid properties were investigated computationally by means of LES and a zonal Hybrid LES/RANS (HLR) method. The latter scheme couples a RANS (Reynolds-Averaged Navier-Stokes) model with large-eddy simulation (LES) within a two-layer framework. A differential near-wall eddy-viscosity model resolves the wall layer and the LES model the remainder of the flow domain. As an introductory heat-transfer case a fully-developed channel flow at Re number $Re_m = 24000$ (DNS: Abe et al., 2004) was computed. In both presently investigated BFS cases the flow is subjected to increasingly enhanced wall heating. Whereas the first considered case ($Re_H = 28000$, $ER = 1.25$), treated experimentally by Vogel and Eaton (1985) - reference LES is due to Keating et al., 2004, deals with a passive scalar transport, the high-intensity heat flux introduced into the flow domain through the step wall in the second investigated configuration ($Re_H = 5540$, $ER = 1.5$; reference LES by Avancha and Pletcher, 2002; corresponding isothermal experiment by Kasagi and Matsunaga, 1995) leads to large temperature gradients causing a strong variation of the flow properties. An important feature of the latter flow is a substantial increase of the friction coefficient magnitude with the wall heating intensification in both the flow reversal and recovery region, associated with the local flow acceleration in the immediate wall vicinity. The results obtained by the present simulations with respect to the mean velocity and temperature fields, friction factor and Stanton number variations follow closely the reference experimental and LES databases.

INTRODUCTION

Turbulent flow over a backward-facing step is one of the most frequently encountered flow configurations in technical practice. A large number of relevant experimental and computational studies can be found in the published literature. Despite its geometrical simplicity, this flow exhibits a number of interesting features, and has served as a popular test case for studying flow separation, reattachment and recovery as well as the influence of the local streamline curvature and adverse pressure gradient. The flow separates at the step edge, forming a highly unsteady, curved shear layer which impinges and bifurcates at the reattachment region; one branch flowing back creates mean and secondary recirculation zones behind the step, another branch creates a new boundary layer downstream. The important prerequisite for successful computation of the flow in the whole is the

*Address all correspondence to this author.

accurate capturing of the near-wall turbulence, characterized by strong Reynolds-stress and stress-dissipation anisotropy. Unlike the flows separated from continuous curved surfaces characterized by highly intermittent separation region whose oscillations spread over a substantial portion of the wall, the backward-facing step flow, characterized by a fixed separation point, can be reasonably well solved by an advanced RANS model. This is in particular related to the size of the recirculation zone. However, the near-wall velocity field in the separation bubble and the consequently lower negative peak of the skin-friction as well as the lower turbulence activity in the separated shear layer represent the common outcome, even after employment of a differential, near-wall Reynolds stress model. The deviation from equilibrium conditions in the backward-facing step configuration is further enhanced by strong temperature gradients (encountered e.g. in gas combustors, heat exchangers, etc.). The influence of strong heating is primarily manifested through a severe variation of the fluid properties (density, viscosity) leading consequently to significant structural changes in the turbulence field. The strongest modification of the flow structure occurs in the inner part of the temperature layer.

The main objective of this work is to validate the present two-layer hybrid LES/RANS method coupling a near-wall $k-\varepsilon$ RANS model with an LES in the outer layer in separated flows with strong property variations due to intensive wall heating. Special attention was devoted to the coupling of both methods, the issue being closely connected to the treatment at the interface separating RANS and LES sub-regions. Hereby, great importance is attached to simplicity, efficiency and applicability to complex geometries. The exchange of the variables across the LES/RANS interface was adjusted by implicit imposition of the condition of equality of the modelled turbulent viscosities (by assuming the continuity of their resolved contributions across the interface), enabling a smooth transition from RANS layer to the LES sub-region. Here, the solutions of the model equations for the RANS quantities (kinetic energy of turbulence and its dissipation rate) merge with the SGS values estimated in line with the Masson and Callen's (1986) proposal for the case of the Smagorinsky model. In addition, a special forcing technique, which compensates the loss of information due to strong damping in the RANS region by creation of artificial and correlated fluctuations, was applied at the interface. This procedure reduces to a large extent the velocity mismatch typically encountered in the interface region. The last issue is the utilisation of a dynamic, flow-dependent interface position in the course of the simulation. A control parameter representing the ratio of the modelled (SGS) to the total turbulent kinetic energy in the LES region, averaged over all grid cells at the interface on the LES side, is adopted in the present work. A typical value of 20% was adopted, corresponding approximately to the reference value an LES resolution should comply with (Pope, 2000). The present hybrid model has been intensively validated in the past in configurations of different geometrical complexity featured by flow separation from sharp-edged and continuous curved surfaces.

COMPUTATIONAL MODEL

The continuity, momentum and energy equations governing the three-dimensional, unsteady flow and heat transfer under the variable property conditions read:

$$\frac{\partial \overline{\rho}}{\partial t}+\frac{\partial(\overline{\rho}\widetilde{U}_i)}{\partial x_i}=0 \tag{1}$$

$$\frac{\partial\left(\overline{\rho}\widetilde{U}_i\right)}{\partial t}+\frac{\partial\left(\overline{\rho}\widetilde{U}_j\widetilde{U}_i\right)}{\partial x_j}=-\frac{\partial \overline{p}}{\partial x_i}+\frac{\partial}{\partial x_j}\left(\overline{\tau}^{\mu}_{ij}+\overline{\tau}^{t}_{ij}\right) \tag{2}$$

$$\frac{\partial\left(\overline{\rho}C_p\widetilde{T}\right)}{\partial t}+\frac{\partial\left(\overline{\rho}C_p\widetilde{U}_j\widetilde{T}\right)}{\partial x_j}=\frac{\partial}{\partial x_j}\left(\overline{q}^{\mu}_{j}+\overline{q}^{t}_{j}\right) \tag{3}$$

Here $\overline{\tau}^{\mu}_{ij}$ $(=2\overline{\mu}\widetilde{S}_{ij}-2\overline{\mu}\widetilde{S}_{kk}\delta_{ij}/3;\ \widetilde{S}_{ij}=0.5(\partial\widetilde{U}_i/\partial x_j+\partial\widetilde{U}_j/\partial x_i))$ and $\overline{q}^{\mu}_{j}$ $(=\overline{\lambda}\partial\widetilde{T}/\partial x_j$; with $\overline{\lambda}=C_p\overline{\mu}/Pr)$ represent viscous stress tensor and viscous heat flux, whereas turbulent stress tensor $\overline{\tau}^{t}_{ij}$ and turbulent heat flux $\overline{q}^{t}_{j}$ are to be modelled (see the following subsections). It is noted, that the term $\overline{\tau}^{\mu}_{ij}\widetilde{S}_{ij}$ denoting the (viscous) dissipation function is omitted in the energy equation. Its contribution is negligible at low Mach numbers applied in the present work. In these equations the overbar ($\overline{\Phi}$) and the tilde ($\widetilde{\Phi}$) denote the standard (Reynolds) and the mass weighted (Favre) averages ($\widetilde{\Phi}\equiv\overline{\rho\Phi}/\overline{\rho}$), respectively. The temperature dependence on viscosity μ and heat conductivity λ is defined via a power-law formulation, while Prandtl number Pr and specific heat at constant pressure C_p were kept constant.

$$\overline{\mu}=\mu_{ref}\left(\frac{\widetilde{T}}{T_{ref}}\right)^{0.71}\quad;\quad\overline{\lambda}=\lambda_{ref}\left(\frac{\widetilde{T}}{T_{ref}}\right)^{0.71} \tag{4}$$

Density is evaluated from the equation for ideal gas $\overline{\rho}=\overline{P}/(R\widetilde{T})$, with R denoting the universal gas constant.

In order to illustrate important issues related to the merging of a near-wall RANS model with conventional LES at a discrete interface the results of the simulations of the flow and heat transfer in a plane channel at a moderate Reynolds number $Re_m=22000$ ($Re_\tau=640$; DNS: Abe et al., 2004) are interactively discussed in the following section. The dimensions of the

computational domain adopted were $(L_x, L_y, L_z) = (2\pi h, 2h, \pi h)$ with $2h$ being the channel height, Fig. 1. Periodic boundary conditions were used in both homogeneous directions x and z. The computations with the reference LES (using dynamic Smagorinsky model) have been performed using the grid $(N_x, N_y, N_z) = (96, 128, 144)$. The computations with the hybrid model and complementary LES (using the standard Smagorinsky model) have been performed on the eight times coarser grid $(48, 64, 72)$ and the thirty two times coarse grid $(24, 64, 36)$.

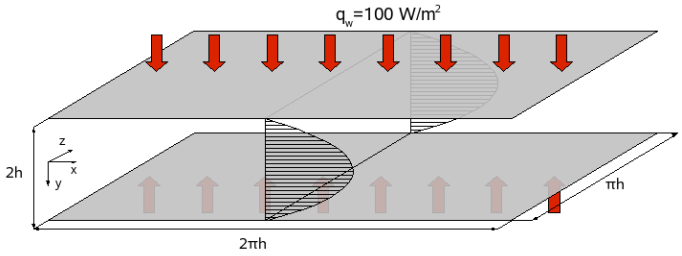

FIGURE 1. Schematic of the channel flow configuration considered

Hybrid LES/RANS model

In the present hybrid LES/RANS formulation, the RANS, i.e. Unsteday RANS (URANS) model covers the near-wall region and the LES model the remainder of the flow domain. The unsteadiness in the RANS sub-region is largely caused by the intensive interaction with the unsteady LES flow field. Both methods share the same temporal resolution. The mass-weighted equations governing the velocity (Eq. 2) and temperature (Eq. 3) fields operate as the Reynolds-averaged Navier-Stokes equations in the near-wall layer ($\widetilde{U}_i$ and $\widetilde{T}$ represent the mass-weighted, ensemble-averaged velocity and temperature fields U_i and T) or as the filtered Navier-Stokes equations in the outer layer ($\widetilde{U}_i$ and $\widetilde{T}$ represent the mass-weighted, spatially filtered velocity and temperature fields). The turbulent stress tensor $\overline{\tau}^t_{ij}$ in Eq. (2) representing either the subgrid-stress tensor ($-\overline{\rho}\,\overline{\tau}_{ij}$) or the Reynolds-stress tensor ($-\overline{\rho}\widetilde{u''_i u''_j}$) is expressed in terms of the mean strain tensor $\widetilde{S}_{ij}$ via the Boussinesq relationship:

$$\overline{\tau}^t_{ij} \equiv -\overline{\rho}\,\overline{\tau}_{ij} = \overline{\mu}_t \left(\frac{\partial \widetilde{U}_i}{\partial x_j} + \frac{\partial \widetilde{U}_j}{\partial x_i} - \frac{2}{3}\frac{\partial \widetilde{U}_k}{\partial x_k}\delta_{ij} \right) - \frac{1}{3}\overline{\rho}\,\overline{\tau}_{kk}\delta_{ij} \quad (5)$$

$$\overline{\tau}^t_{ij} \equiv -\overline{\rho}\widetilde{u''_i u''_j} = \overline{\mu}_t \left(\frac{\partial \widetilde{U}_i}{\partial x_j} + \frac{\partial \widetilde{U}_j}{\partial x_i} - \frac{2}{3}\frac{\partial \widetilde{U}_k}{\partial x_k}\delta_{ij} \right) - \frac{2}{3}\overline{\rho}\tilde{k}\delta_{ij} \quad (6)$$

with $\tilde{k} = 0.5\widetilde{u''_i u''_i}$.

The turbulent heat flux $\overline{q}^t_i$ in the equation governing the temperature field is modelled by using the simple gradient diffusion hypothesis

$$\overline{q}^t_i = -\overline{\rho} C_p \widetilde{u_i \theta} = \overline{\lambda}_t \frac{\partial \widetilde{T}}{\partial x_i} \text{ with } \overline{\lambda}_t = \frac{\overline{\mu}_t C_p}{Pr_t} \quad (7)$$

The equations governing the velocity and temperature field in the hybrid LES/RANS framework are:

$$\frac{\mathbf{D}(\overline{\rho}\widetilde{U}_i)}{\mathbf{D}t} = -\frac{\partial \overline{p}^*}{\partial x_i} + \frac{\partial}{\partial x_j}\left[(\overline{\mu} + \overline{\mu}_t)\left(\frac{\partial \widetilde{U}_i}{\partial x_j} + \frac{\partial \widetilde{U}_j}{\partial x_i} - \frac{2}{3}\frac{\partial \widetilde{U}_k}{\partial x_k}\delta_{ij} \right) \right] \quad (8)$$

$$\frac{\mathbf{D}(\overline{\rho}\widetilde{T})}{\mathbf{D}t} = \frac{\partial}{\partial x_j}\left[\left(\frac{\overline{\mu}}{Pr} + \frac{\overline{\mu}_t}{Pr_t} \right)\left(\frac{\partial \widetilde{T}}{\partial x_j} \right) \right] \quad (9)$$

As usual, the isotropic parts of the stress tensors ($\overline{\rho}\,\overline{\tau}_{kk}\delta_{ij}/3$ and $2\overline{\rho}\tilde{k}\delta_{ij}/3$) are grouped together with the pressure in the equations of motion: $\overline{p}^* = \overline{p} + \overline{\rho}\,\overline{\tau}_{kk}/3$ (if Eqs. 2 operate as the filtered Navier-Stokes equations in the outer layer) and $\overline{p}^* = \overline{p} + 2\overline{\rho}\tilde{k}/3$ (if Eqs. 2 operate as the Reynolds-averaged Navier-Stokes equations in the near-wall layer).

In the present two layer hybrid LES/RANS scheme the coupling of the instantaneous LES field and the ensemble-averaged RANS field at the interface is realized via the turbulent viscosity, which makes it possible to obtain solutions using one system of equations. This means practically that the governing equations (8) and (9) are solved in the entire solution domain irrespective of the flow sub-region (LES or RANS). Depending on the flow zone, the hybrid model implies the determination of the turbulent viscosity $\overline{\mu}_t$ either from a $k-\varepsilon$ RANS model: $\overline{\mu}_t = \overline{\rho} C_\mu f_\mu k^2/\varepsilon$ or from the LES formulation: $\overline{\mu}_t = \overline{\mu}_{SGS} = \overline{\rho}(C_S\Delta)^2|\widetilde{S}|$. The Smagorinsky constant C_S takes the value of 0.1. $\Delta = (\Delta x \times \Delta y \times \Delta z)^{1/3}$ represents the filter width and $|\widetilde{S}| = (\widetilde{S}_{ij}\widetilde{S}_{ij})^{1/2}$ the strain rate modulus.

The near-wall variation of the turbulent viscosity $\overline{\mu}_t$ is obtained from a $k-\varepsilon$ RANS model implying solving of the following two transport equations:

$$\frac{\mathbf{D}(\overline{\rho}\tilde{k})}{\mathbf{D}t} = \frac{\partial}{\partial x_j}\left[\left(\overline{\mu} + \frac{\overline{\mu}_t}{\sigma_k} \right)\frac{\partial k}{\partial x_j} \right] + \overline{\rho}\,\mathscr{P}_k - \overline{\rho}\varepsilon \quad (10)$$

$$\frac{\mathbf{D}(\overline{\rho}\varepsilon)}{\mathbf{D}t} = \frac{\partial}{\partial x_j}\left[\left(\overline{\mu} + \frac{\overline{\mu}_t}{\sigma_\varepsilon} \right)\frac{\partial \varepsilon}{\partial x_j} \right] + \overline{\rho}\frac{C_{\varepsilon,1}\mathscr{P}_k - f_\varepsilon C_{\varepsilon,2}\varepsilon}{\tau} + \mathscr{P}_{\varepsilon,3} \quad (11)$$

with $\tau = k/\varepsilon$ representing the turbulent time scale. The near-wall and viscous damping functions (f_μ and f_ε) and the production term $\mathscr{P}_{\varepsilon,3}$ (Eqs. 10 and 11), are presently modelled in line with the proposal of Chien (1982) with ε representing the isotropic part of the total viscous dissipation rate taking zero value at the wall.

Because k and ε are not provided (in the case of the subgrid-scale (SGS) model of Smagorinsky) within the LES sub-domain, their SGS values are estimated using the proposal of Mason and Callen (1986):

$$k_{SGS} = \frac{(C_S\Delta)^2|\widetilde{S}|^2}{0.3} \text{ and } \varepsilon_{SGS} = (C_S\Delta)^2|\widetilde{S}|^3 \qquad (12)$$

The RANS equations for k and ε are solved in the entire flow field, but with the discretization coefficients taking zero values in the LES sub-region. By manipulating appropriately the source terms, the numerical solution of these equations in the framework of the finite volume method provides the interface values of the k_{RANS} and ε_{RANS} being equal to the corresponding SGS values. By doing so, the boundary condition at the LES/RANS interface (*ifce*) implying the equality of the modelled turbulent viscosities (by assuming the continuity of their resolved contributions across the interface, Temmerman et al., 2005) at both sides of the interface:

$$\overline{\mu}_{t,ifce}|_{RANS-side} = \overline{\mu}_{t,ifce}|_{LES-side}$$

is implicitly imposed without any further adjustment, see Fig. 2 for illustration. In such a way a smooth transition of the turbulent viscosity is ensured.

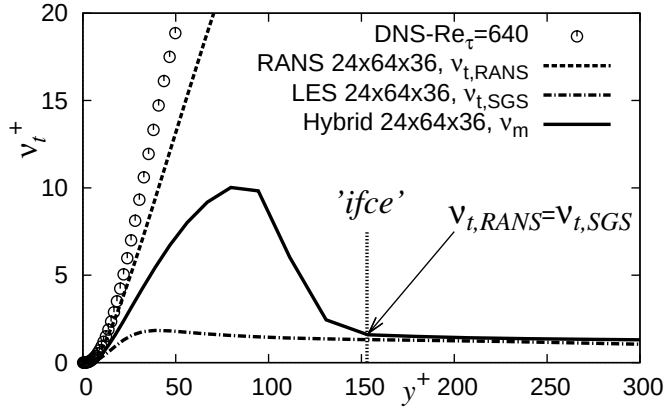

FIGURE 2. Variation of modelled turbulent viscosity across the interface in a fully-developed channel flow

One of the advantages of a zonal approach is the possibility to predefine the LES-RANS interface. However, in unknown flow configurations, this could be a difficult issue. Therefore, a certain criteria expressed in terms of a control parameter should be introduced. Presently, the following control parameter

$$k^* = \left\langle \frac{k_{mod}}{k_{mod} + k_{res}} \right\rangle \qquad (13)$$

is adopted, representing the ratio of the modelled (SGS) to the total turbulent kinetic energy in the LES region, averaged over all grid cells in homogeneous direction at the interface on the LES side. As soon as this value exceeds 20 %, the interface is moved farther from the wall and in opposite direction when the value goes below 20 %. This additionally ensures that in the limit of a very fine grid (very low level of the residual turbulence) LES is performed in the most of the solution domain. In contrast, in the case of a coarse grid, RANS prevails. As the interface separates the near wall region from the reminder of the flow, it would be suitable to choose a wall-defined parameter for denoting the interface location. In the present study, the dimensionless wall distance y^+ was adopted. Despite possible difficulties in respect to the definition of y^+ in flow domains where the wall shear stress approaches zero, as e.g. in separation and reattachment regions, no problems in the course of the computations have arisen (one may recall that the same non-dimensional wall distance y^+ is regularly used in the van Driest's wall-damping of μ_t also in LES of separating and reattaching flows). It is noted, that the interface y^+ doesn't represent a model parameter in the HLR method. It only denotes the computational nodes at which the prescribed value of k^* is obtained. For illustration see Fig. 3 displaying a snapshot of the instantaneous velocity field with the corresponding evolution of the averaged interface value along the upper wall and the lower (step) wall in the backward-facing step flow investigated experimentally by Kasagi and Matsunaga (1995).

A typical outcome of the application of a zonal (it is also pertinent to some seamless methods, as e.g. DES method - Detached Eddy Simulation, e.g. Nikitin et al., 2000) hybrid LES/RANS method is the formation of a kind of buffer layer aligned with the region around interface separating the RANS sub-region from the LES one. This buffer layer represents one important problem reported in just about all relevant publications. The lack of proper resolution of the near-wall streaky structure, which cannot be fully compensated by modelling, leads to unphysical effects. The modelled turbulence, provided by the RANS and LES SGS on the two sides of the interface differ significantly, whereas the resolved contribution should be the same or close to each other. The turbulence fluctuations (originating from the RANS-region) transferred through the interface do not correspond to those pertinent to the LES sub-region. The relatively high RANS turbulent viscosity strongly damps the fluctuations, suppressing their

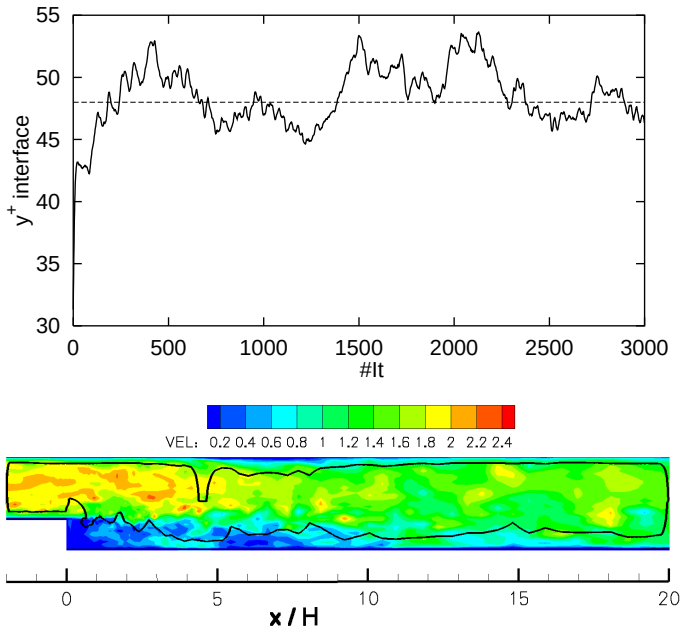

FIGURE 3. Temporal variation of the interface position in terms of dimensional wall distance y^+ (upper) and instantaneous velocity field and the corresponding evolution of the interface value $y^+_{ifce} = 48$ corresponding to the lower wall

recovery until some distance behind the interface. Closely connected to this phenomenon is an unphysical bump at the mean velocity profile, as well as at the mean temperature profile, at the distance corresponding to the interface position. This is especially visible in computations of wall-attached flows where there is no dominating forcing (e.g. channel flows), Figs. 4 (dashed lines). Several earlier investigations have shown that one can diminish or even eliminate this bump by adding some additional forcing in form of variable fluctuations in the interface region. Such a 'forcing' procedure, introduced by Piomelli et al. (2003), acts towards the acceleration of the fluctuations recovery at the LES side. Hereby, the important issues are the type and intensity of these synthetic fluctuations. A relevant method, implying the generation of the fluctuations whose spatial and temporal extent corresponds to the given filter width and time step respectively, which originates from a digital-filter-based generation of inflow data for spatially developing DNS and LES due to Klein et al. (2003) was adopted in the present work. This method, being originally developed to work at an inflow plane meshed by a 2-D, Cartesian equidistant grid (a prescribed correlation function for isotropic turbulence was applied), was presently extended to comply with non-orthogonal grids and irregular interface shapes, see e.g. Fig. 3. Its use increases the computational costs to some extent. However, it should be emphasized that the fluctuations are computed only at the interface. The common procedure for generating the pseudo-turbulent velocity field implies the superimposition of a field of random fluctuations to the mean velocity field. The velocity fluctuations are to be obtained by appropriate transformation of stochastic signals in a way to get reproduced the background Reynolds stress tensor. The starting point are the time-averaged profiles of the mean velocity and Reynolds stress components, which are to be provided by applying the RANS model, being anyhow the constitutive part of a hybrid LES/RANS method. This approach is therefore regarded as especially suitable for the present problem. The steps to be performed are summarized as follows: 1. creation of random fluctuations, 2. filtering of fluctuations in space and time, 3. adjustment to local Reynolds stresses and 4. introduction into momentum equations through a source term The strength of the forcing depends on the interface position. The closer the interface is to the wall, the less forcing is needed. Two important observations emerged. First, it seems sufficient to introduce forcing only into the equations governing the velocity field, which also reduces the bump in the mean temperature profile. Second, the forcing is needed only in the direction normal to the interface. Herewith, the recovery of the fluctuations on the LES side of the interface is accelerated and the afore-mentioned velocity and temperature bumps are eliminated to a largest extent, Figs. 4 (solid lines).

Fig. 5 shows the profiles of the total k, which were obtained by summing up the resolved and modelled parts. The modelled part is determined by the model used and the resolved part resulted from the averaging of the instantaneous velocity fields over a certain time period. Due to unsteady treatment of the RANS layer and the RANS field excitation by the adjacent instantaneous LES field through the interface, one can observe a resolved part also in this region. The modelled part clearly diminishes when crossing the interface. Fig. 5 illustrates also the effects of the interface turbulence forcing on the profile of the kinetic energy of turbulence. The reduction of the modelled fraction and increase of the resolved turbulent kinetic energy within the RANS layer are obvious. Simply said, the damping effect of the RANS layer on the LES sub-region is appropriately weakened. One can still note a certain kink at the both profiles (noticeable also at Reynolds stress component profiles, Figs. 6), which originates by largest extent from the resolved part. However, this fact does not influence the computational procedure.

All three normal Reynolds stress components, depicted in Fig. 6, are correctly captured (apart of the incorrect asymptotic behaviour of the normal-to-wall component), despite the use of the linear $k-\varepsilon$ model due to Chien (1982) in the near-wall RANS layer, known to result in a completely isotropic situation in the fully-developed channel flow: $\overline{u^2} = \overline{v^2} = \overline{w^2} = 2k/3$.

It is clearly visible that the HLR method with forcing performs better than the corresponding coarse LES. The results obtained are even very close to the fine LES. The computational

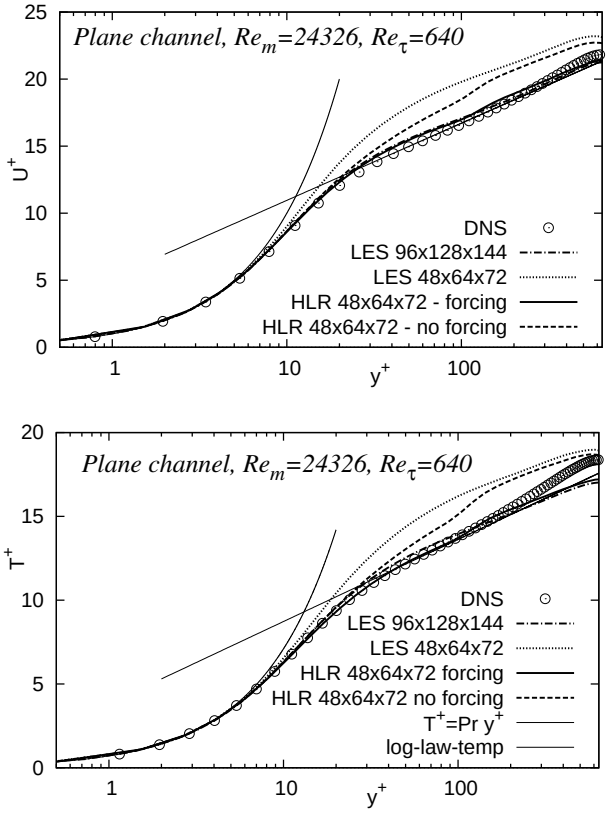

FIGURE 4. Semi-log plot of mean velocity and mean temperature profile across a fully-developed channel flow: effect of turbulence forcing in the interface region.

costs of HLR in this channel flow exceeds those of the coarse LES by about 30% due to the solving of additional equations for k and ε and activated forcing procedure.

Numerical method All computations were performed with the in-house computer code FASTEST based on a finite volume numerical method for solving both the three-dimensional filtered and Reynolds-averaged Navier-Stokes equations on block structured, body fitted, non-orthogonal meshes. Block interfaces are treated in a conservative manner, consistent with the treatment of the inner cell faces. A cell centered (collocated) variable arrangement and Cartesian vector and tensor components are used. The well-known SIMPLE algorithm is applied for coupling the velocity and pressure fields. The convective terms in all equations are discretized by a second-order central differencing scheme (CDS), whose stability is enhanced by the deferred correction approach (see e.g., Khosla and Rubin, 1974). The time discretization is accomplished applying the second order (implicit) Crank-Nicolson method.

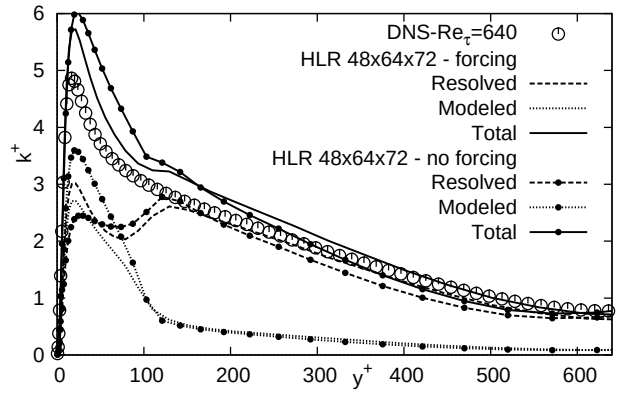

FIGURE 5. Kinetic energy of turbulence profile across a fully-developed channel flow: effect of turbulence forcing in the interface region.

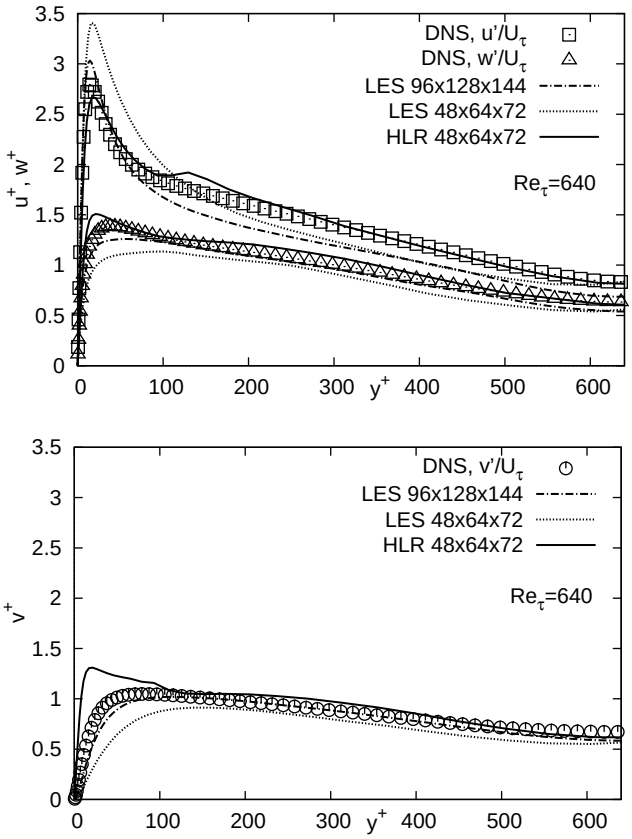

FIGURE 6. Normal Reynolds stress components across a fully-developed channel flow: effect of turbulence forcing in the interface region.

FLOW CONFIGURATIONS CONSIDERED

Schematic of the backward-facing step (BFS) flow configuration indicating the domain of interest is displayed in Fig. 7. The boundary layer at the step-wall separates at the step edge (fixed separation point) and reattaches at the bottom wall building the recirculation zone immediately behind the step. The bottom wall downstream of the step was heated by a uniformly supplied heat flux, the latter representing the thermal boundary conditions.

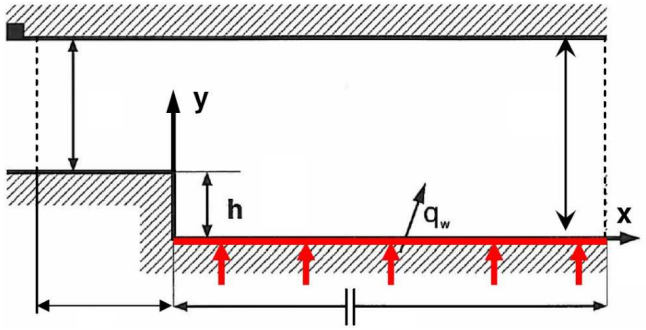

FIGURE 7. Schematic of flow configuration considered

BFS flow: constant fluid properties The experimental database is provided by Vogel and Eaton (1985). The flow Reynolds number based on the step height ($H = 0.038\,m$) and the upstream centerline velocity ($U_c = 11.3\,m/s$) is $Re_H = 28000$. The upstream flow conditions correspond to a developing flow in a channel of height $4H$. The boundary layer developing at lower wall separates at the step edge transforming into the separated shear layer within the expanded channel section of height $5H$. Accordingly, the expansion ratio ER is 1.25. The boundary layer thickness at the step edge is approximately equal to the step height $\delta = 1.0658H$. The relevant momentum thickness is $\theta = 4.68\,mm$ and the corresponding Reynolds number $Re_\theta = 3370$. The fluid properties adopted from the experimental investigations are: $\rho = 1.225\,kg/m^3$, $\nu = 1.54410^{-5}\,m^2/s$, $C_p = 1005\,J/(kgK)$, $\lambda = 0.02615\,W/(mK)$ and $Pr = 0.712$. The lower wall in the channel after expansion was heated by the heat flux $q_w = 270\,W/m^2$. All other walls are treated as adiabatic. The highest temperature increase compared to the inflow is about 6%. Accordingly, the fluid property dependence on the temperature field is negligible. Two LES simulations serving as computational reference in the present work have been performed by Akselvoll and Moin (1995) and Keating et al. (2004). The considered flow domain (Fig. 8) after expansion was extended up to $20H$ in accordance with the latter work. The solution domain adopted for this moderately high Reynolds number backward-facing step flow was discretized by $112 \times 100 \times 64$ grid points (without inlet channel), which is about three times coarser than the grid used in LES of Akselvoll and Moin (1995) and about four times coarser than the Keating's et al. one. The instantaneous inflow corresponding to a boundary layer developing at the step wall was generated by using the method proposed by Klein et al., 2003 (the same procedure was adopted for the forcing technique, section 'Hybrid LES/RANS model'). The mean flow quantities necessary for the inflow generation were provided from the separate boundary-layer computations performed by using the near-wall second-moment closure model of Jakirlic and Hanjalic (2002). The corresponding interface variation is displayed in Figs. 9.

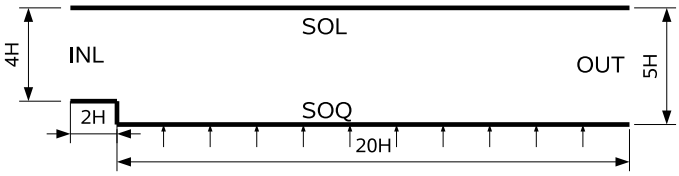

FIGURE 8. Computational domain adopted for the constant property BFS flow simulations

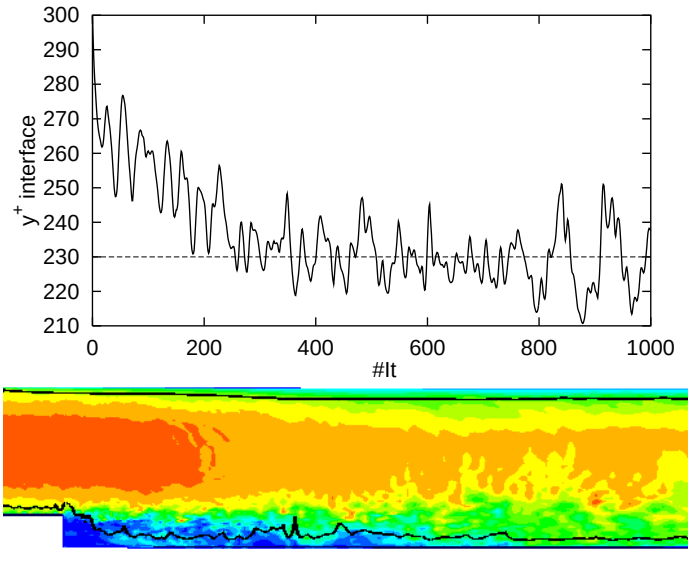

FIGURE 9. Temporal variation of the interface position in terms of dimensional wall distance y^+ (upper) and instantaneous velocity field and the corresponding evolution of the interface value $y^+_{ifce} = 230$ corresponding to the lower wall

BFS flow: variable fluid properties The flow Reynolds number based on the step height ($H = 0.041\,m$) and the upstream centerline velocity ($U = 2.063\,m/s$) is $Re_H = 5540$. The upstream conditions correspond to fully-developed flow in a channel of height $2H$ (inflow was generated by performing precursor channel flow calculations) providing the expansion ratio of $ER = 1.5$. Three cases with increasing wall heat flux ($q_w = 1$, 2 and 3 kW/m^2; reference LES by Avancha, 2001, and Avancha and Pletcher, 2002) were computed in addition to the isothermal flow (Exp.: Kasagi and Matsunaga, 1995). All other flow and fluid properties were adopted from the work of Avancha and Pletcher: $T_{ref} = 293\,K$, $\rho_{ref} = 1.194\,kg/m^3$, $\lambda_{ref} = 0.02574\,W/(mK)$, $\nu_{ref} = \mu_{ref}/\rho_{ref} = 1.527 \times 10^{-5} m^2/s$, $Pr = 0.71$ and $C_p = 1006\,J/(kgK)$. The grid covering the flow domain after expansion (20 step heights, Fig. 10) contains $72 \times 42 \times 40$ cells. The inflow plane was positioned at two step heights upstream from the step edge. This inlet region was meshed with additional $14 \times 28 \times 40$ grid cells, resulting in about 136.000 cells in total. Precursor simulation of the fully-developed channel flow ($Re_\tau \approx 290$) was performed in order to generate appropriate inflow. The interface development corresponds approximately to the one displayed in Fig. 3 with $y^+_{ifce} \approx 48$. The grid used by Avancha and Pletcher was of comparable size. The same solution domain was meshed by $72 \times 46 \times 48$ cells downstream of the step and $17 \times 31 \times 48$ cells upstream of the step resulting in about 184.000 cells in total.

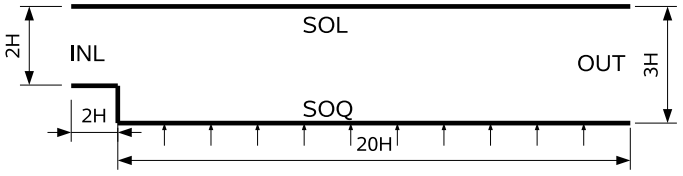

FIGURE 10. Computational domain adopted for the variable property BFS flow simulations

RESULTS AND DISCUSSION

Some selected results obtained by the present hybrid LES/RANS model (denoted by HLR) for both the constant fluid properties flow and the cases involving severe property variations due to the strong wall heating are shown and discussed in the next subsections along the reference experimental (Kasagi and Matsunaga, 1995; Vogel and Eaton, 1985) and reference LES (Avancha, 2001 and Avancha and Pletcher, 2002) database. In addition, the results obtained by the conventional LES method using the SGS model of Smagorinsky and the same grid resolution as in the case of the HLR model scheme are also displayed. These 'coarse' LES results are denoted by LESc.

Backward-facing step flow and heat transfer with constant fluid properties

Figs. 11 show the evolution of the mean axial velocity and the streamwise turbulence intensity profiles at selected streamwise locations. The HLR model returned somewhat higher backflow intensity. Other results exhibit very good mutual agreement as well as agreement with available experimental data. Additional large-eddy simulation was performed using the same grid. The variable interface method (Eq. 13) was applied (see Figs. 9 and 3 and appropriate discussion for more details).

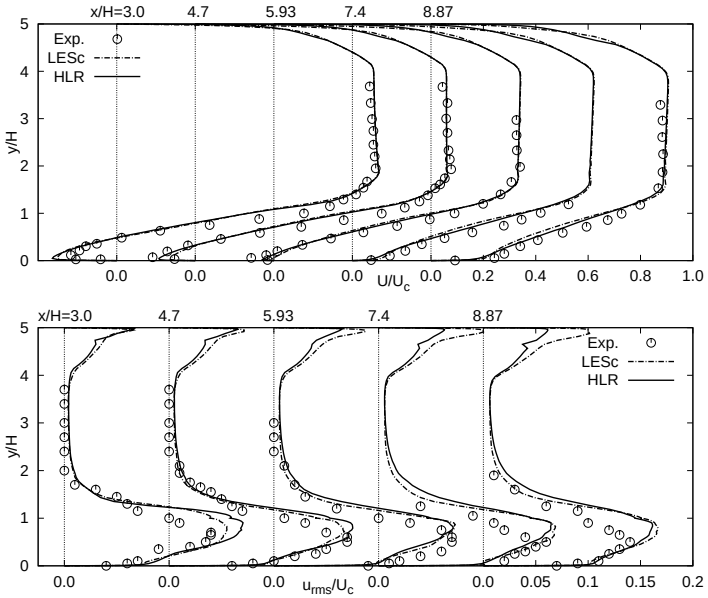

FIGURE 11. Mean axial velocity and streamwise turbulence intensity profiles at selected locations in the constant fluid property backward-facing step flow

The results of the reattachment length obtained by several computational methods and experiment are summarized in Table 1. The HLR results are very close to the experimental finding and to the results obtained by dynamic Smagorinsky model (Akselvoll and Moin, 1995). Remarkable are the deviations of the LES results obtained on the same, relatively coarse grid and especially of the Chien $k-\varepsilon$ model results. It is interesting to note, that just these two models represent the constitutive parts of the present HLR method.

Figs. 12 display the development of the profiles of the mean temperature and temperature variance at several streamwise locations. Some deviations of the computed temperature field from

TABLE 1. Comparison of reattachment lengths obtained by the present HLR model and available experimental and computational results

	Reattachment length	Grid points $[10^6]$
Experiment	$6.70H$	-
LES (Dyn., Akselvoll and Moin)	$6.74H$	2.25
LES (Dyn., Keating et al.)	$6.54H$	1.30
LES coarse (Smag.)	$6.30H$	0.76
Hybrid LES/RANS	$6.78H$	0.76
Chien's low-Re $k-\varepsilon$	$5.87H$	0.012

the reference experiment are noticeable only immediately behind the step (locations x/H=0.33 and 1.67). The results at other locations exhibit very good agreement with available experimental data.

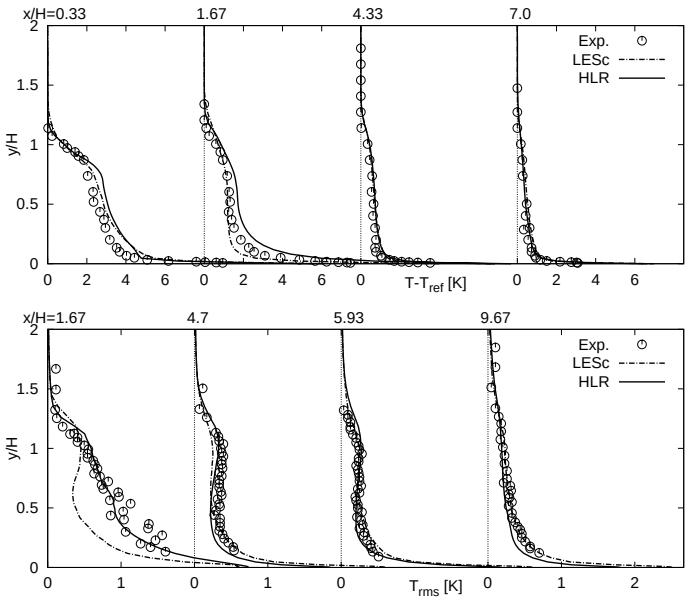

FIGURE 12. Profiles of mean temperature and temperature variance at selected locations in the constant fluid property backward-facing step flow

The evolutions of the friction coefficient C_f and Stanton number St along the lower wall, Fig. 13, obtained by the HLR model follow closely the experimental ones apart of somewhat overpredicted C_f in both recirculation (negative peak) and recovery regions and underpredicted Stanton number in the recovery region.

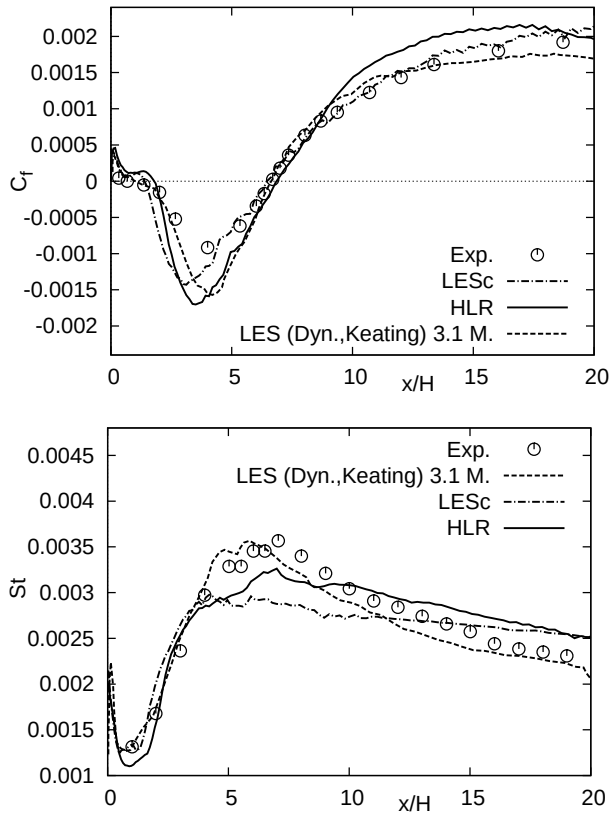

FIGURE 13. Friction fraction and Stanton number evolutions in the constant fluid property backward-facing step flow

Backward-facing step flow and heat transfer with variable fluid properties

The comparison of the mean streamline patterns in the recirculation region pertinent to the isothermal case, Fig. 14, shows that the present hybrid LES/RANS schemes yields the reattachment length of $x_r/H = 6.9$, somewhat larger compared to the experimental one $x_r/H = 6.51$. A similar discrepancy applies also to the corner bubble. The same conclusion can be deduced from the friction factor shown in Fig. 15. In contrast, the result of Avancha (2001) indicates a zero C_f at $x_r/H \approx 5.4$ (though the reattachment length quoted explicitly was $x_r/H = 6.1$). It is difficult to judge the credibility of the latter finding in the absence

of appropriate measurements (C_f evolution was not available in the experimental database of Kasagi and Matsunaga). Because of that, the results of some other experimental (Jovic and Driver, 1993) and computational studies (DNS: Le et al., 1997; LES: Saric et al., 2005) of the backward-facing step configurations at comparable flow Reynolds numbers (Re_H) and expansion ratios (ER) are also displayed in Fig. 15. The C_f-evolution obtained by the HLR model agrees reasonably with these results with respect to both the main and secondary reattachment lengths, in contrast to the LES results of Avancha and Pletcher, which report both lengths to be substantially shorter. Furthermore, the negative peak value is too high and the C_f-evolution in the recovery region indicates a significant underprediction. Also, these results show some curious behaviour immediately after expansion, such as high positive values at the separation point $x/H = 0$, where, per definition, C_f should take zero value. Fig. 16 displays

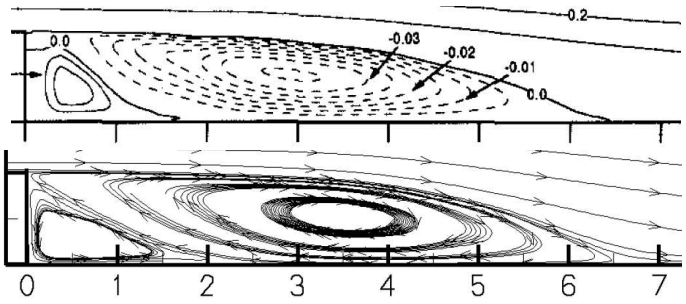

FIGURE 14. Mean streamlines obtained a) experimentally (upper) and applying the present HLR model (lower)

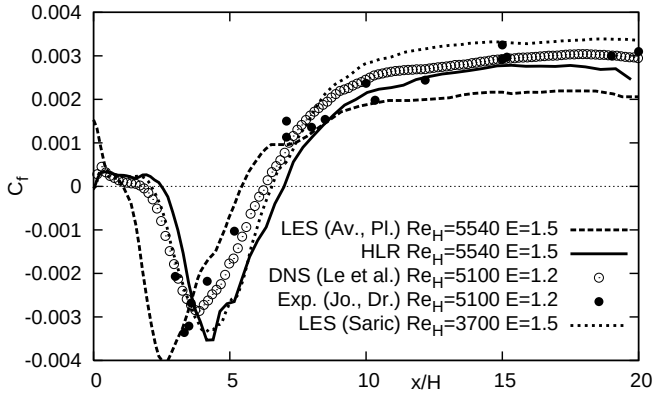

FIGURE 15. Friction coefficient evolution

very good agreement between present computational results and experimental data in all characteristic regions of the backward-facing step configuration.

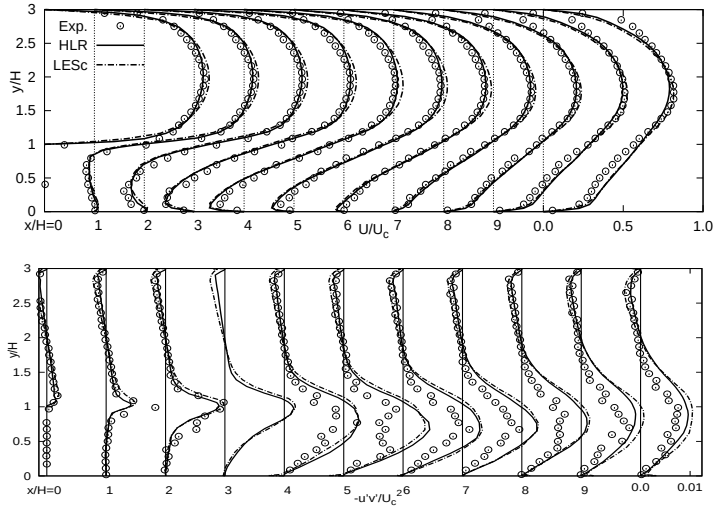

FIGURE 16. Evolution of the mean axial velocity and shear stress component profiles - isothermal case

The simulations of the cases with wall heating were performed for three different wall heat fluxes $q_w = 1$, 2 and $3\,kW/m^2$ (corresponding to the normalized heat flux levels - $Q_w = q_w/(\rho_{ref} C_p U_{ref} T_{ref})$ - of 0.0014, 0.0028 and 0.0042). Fig. 17 depicts the mean temperature evolution for the case with the highest wall heat flux level $q_w = 3\,kW/m^2$. Direct comparison of the mean velocity field (Fig. 18) with the isothermal case (putting the profiles into the same diagram) reveals weak influence of the strong temperature variation on the reattachment length (the same conclusion can be drawn from the C_f evolutions for all three heat flux levels, Fig. 19). The most important changes compared to the isothermal case are concentrated in the region of the secondary recirculation and associated reattachment region as well as in the immediate post-reattachment zone. These differences are manifested through the velocity gradient enhancement characterized by increase of the maximum shear stress. The influence of the strong temperature gradient (the wall temperature for the case with $q_w = 3\,kW/m^2$ takes here the values slightly below $1000\,K$, Figs. 20 and 21) on the flow immediately after expansion is visible in all following diagrams. The C_f evolutions displayed in Fig. 19 reveal a very interesting dependence on the heat flux level supplied. In order to make direct comparison between the reference LES and the present computational results the values on x-axis are normalized with the corresponding reattachment length (see discus-

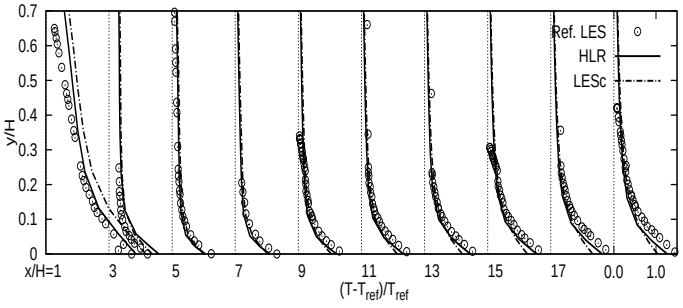

FIGURE 17. Evolution of the mean temperature profiles - $q_w = 3kW/m^2$

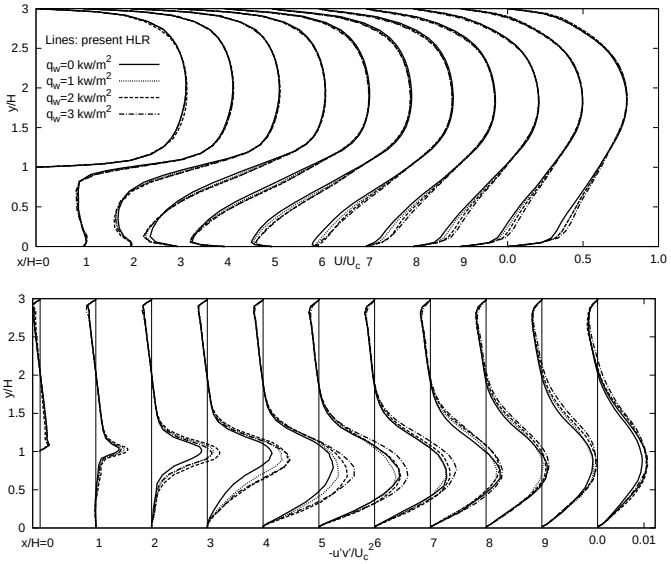

FIGURE 18. Evolution of the mean axial velocity and and shear stress component profiles - $q_w = 0$, 1, 2 and $3kW/m^2$

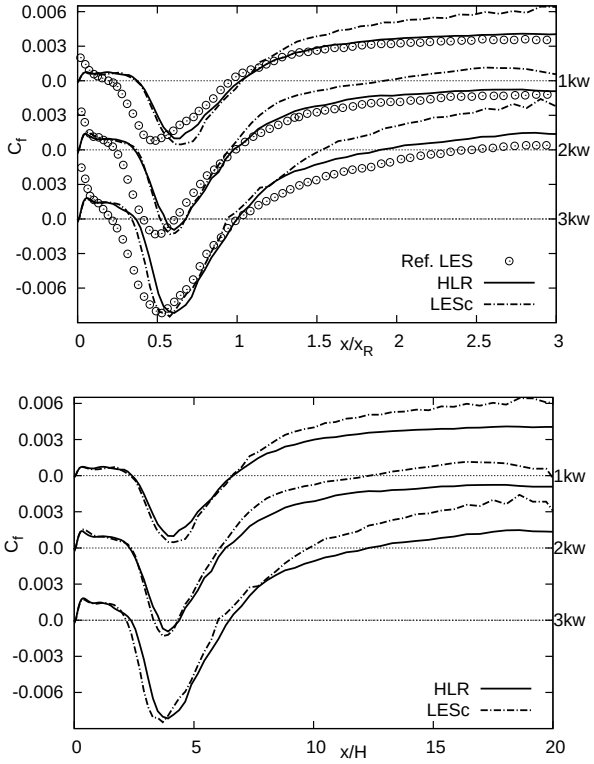

FIGURE 19. Friction coefficient evolution for all three cases with wall heating - $q_w = 1$, 2 and $3kW/m^2$

sion about reattachment length predictions in the previous subsection). The C_f developments are characterized by high negative peaks in the recirculation zone representing a well-known feature characteristic for the lower flow Reynolds number (compare these values with the C_f-development obtained in the Vogel and Eaton case at $Re_H = 28000$). Both the negative peak in the recirculation zone (up to three times higher magnitude compared to the isothermal case) and the positive maximum value in the recovery region (an increase of 100% compared to the case with $q_w = 0$) increase with the heat flux level increase. Such an outcome is pertinent to the intensification of the convective mixing within the separation bubble due to the strong heating. Although less intensive, an analogous acceleration occurs in the immediate wall vicinity within recovery region. The C_f predictions obtained with the reference LES exhibit, similar as in the isothermal flow, unrealistic (high) final values at the fixed separation point $x = 0$; accordingly, they should be handled with caution. Apart of that, the C_f dependence on the heat flux in the recovery region was returned in a very good agreement with the reference LES. The present LES results obtained on the same grid used for the HLR computations exhibit significant overprediction. Both the bulk and the wall temperature variations agree very well with the reference LES. Fig. 22 displays the variation of the coefficient of the dynamic viscosity. As expected, $\overline{\mu}$ reaches its maximum at the position coinciding with the secondary reattachment location, where the backflow in the mean recirculation zone and the (positive) flow within the corner bubble hit each other. A direct comparison with the reference LES data in this region is inadequate because of the reasons explained previously. Both databases exhibit a high level of agreement in the recovery region. The evolution of the Nusselt ($Nu = q_w H/(\lambda_{bulk}(T_w - T_{bulk}))$; $\lambda_{bulk} = \lambda_{ref}(T_{bulk}/T_{ref})^{0.71}$) and Stanton ($St = q_w T_{ref}/(T_w - T_{bulk})$) numbers depicted in Fig. 23 reflects entirely the bulk and wall temperature variations.

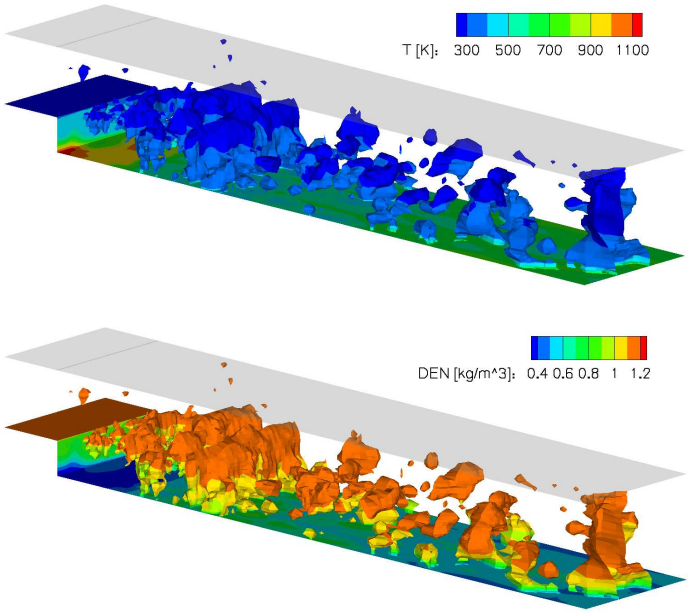

FIGURE 20. Contours of the fluctuating pressure coloured with the instantaneous temperature and density - $q_w = 3kW/m^2$

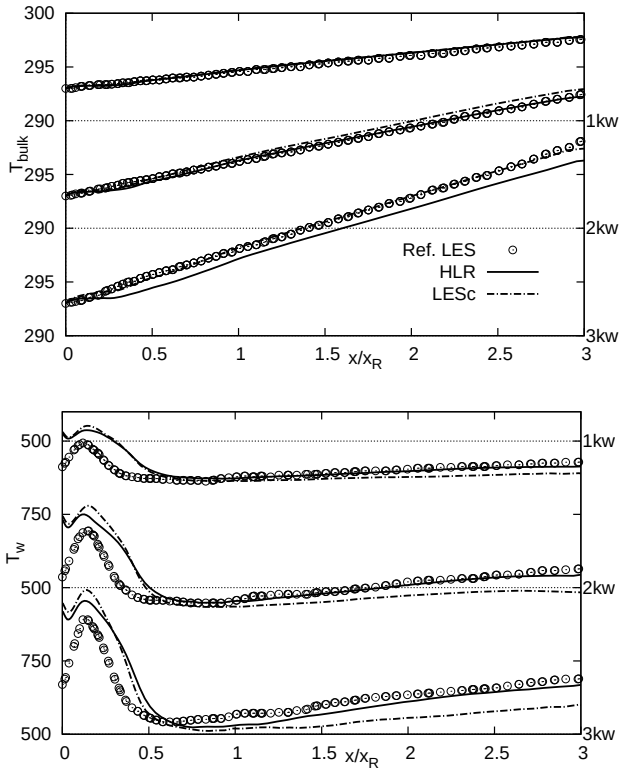

FIGURE 21. Bulk (upper) and wall (lower) temperature variation for all three cases with wall heating - $q_w = 1$, 2 and $3kW/m^2$

CONCLUSIONS

The capability of a newly proposed hybrid LES/RANS model scheme employing low-Reynolds number, eddy-viscosity-based RANS model in the near-wall layer and the Smagorinsky SGS model in the core flow was demonstrated by computing the separating flow behind a backward-facing step involving strong fluid property variation due to uniform heat flux supplied through the bottom wall downstream of the step. A variable interface between RANS and LES regions was applied, whose position was controlled by a parameter corresponding to an in-advance prescribed fraction of kinetic energy of turbulence. The results obtained by the present HLR computational model with respect to the reattachment lengths, C_f and Stanton number evolutions, fluid flow and thermal fields follow closely the reference experiment (Kasagi and Matsunaga, 1995) and reference LES (Avancha and Pletcher, 2002). This is especially the case in the recovery region. The deviations related to the wall temperature and flow property variations, concentrated mostly in the region of the corner bubble immeditelly after sudden expansion, are associated with the inadequate reference LES predictions (Avancha and Pletcher) of the secondary reattachment length. The HLR results are generally superior to the LES data obtained on the same grid.

ACKNOWLEDGMENT

The financial support of the Deutsche Forschungsgemeinschaft through the grant SFB568 "Flow and Combustion in Future Gas Turbine Combustion Chambers" for B. Kniesner is gratefully acknowledged

References

[1] Abe, H., Kawamura, H., and Matsuo, Y., 2004, Surface heat-flux fluctuations in a turbulent channel flow up to Re_τ =1020 with $Pr = 0.025$ and 0.71. *Int. J. Heat and Fluid Flow*, Vol. 25, pp. 404-419

[2] Avancha, R.V.R., 2001, A study of the heat transfer and fluid mechanics of the turbulent separating and reattaching flow past a backward-facing step using large-eddy simulation, Ph.D. Thesis, Iowa State University

[3] Avancha, R.V.R. and Pletcher, R.H., 2002, Large eddy simulation of the turbulent flow past a backward-facing step with heat transfer and property variations, *Int. J. Heat and Fluid Flow*, Vol. 23, pp. 601-614

[4] Chien, K.-Y., 1982, Predictions of Channel and Boundary-Layer Flows with a Low-Reynolds-Number Turbulence

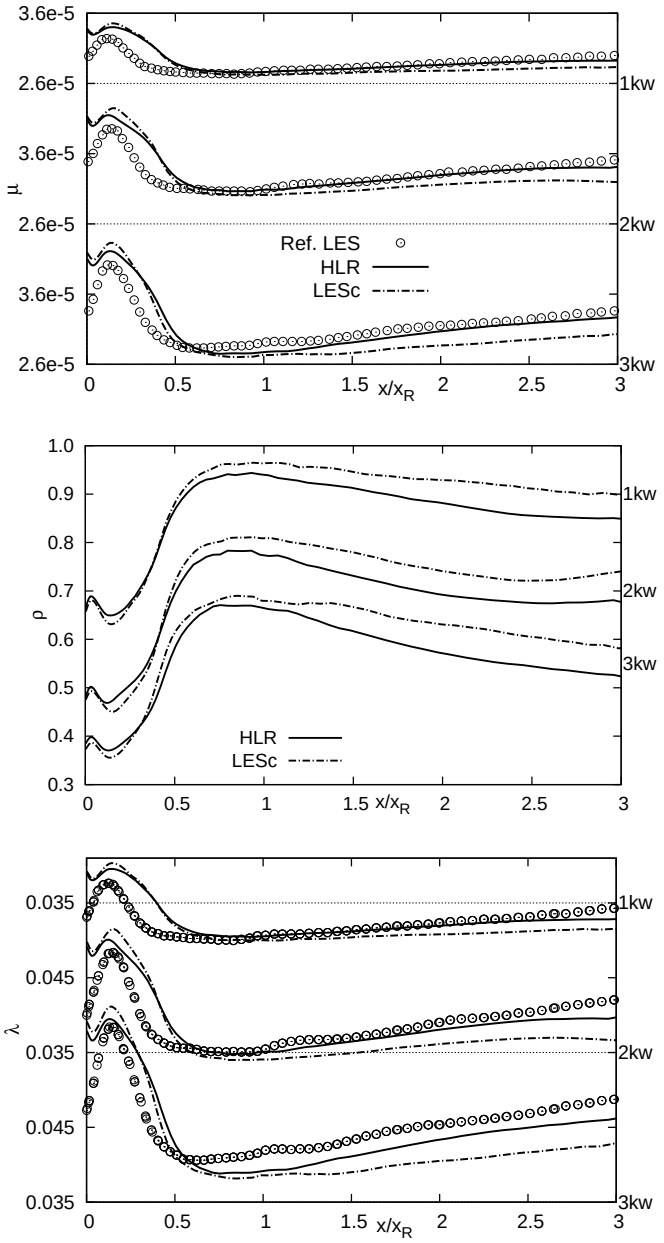

FIGURE 22. Variation of the viscosity (upper), density (middle) and thermal conductivity (lower) for all three cases with wall heating - $q_w = 1$, 2 and $3kW/m^2$

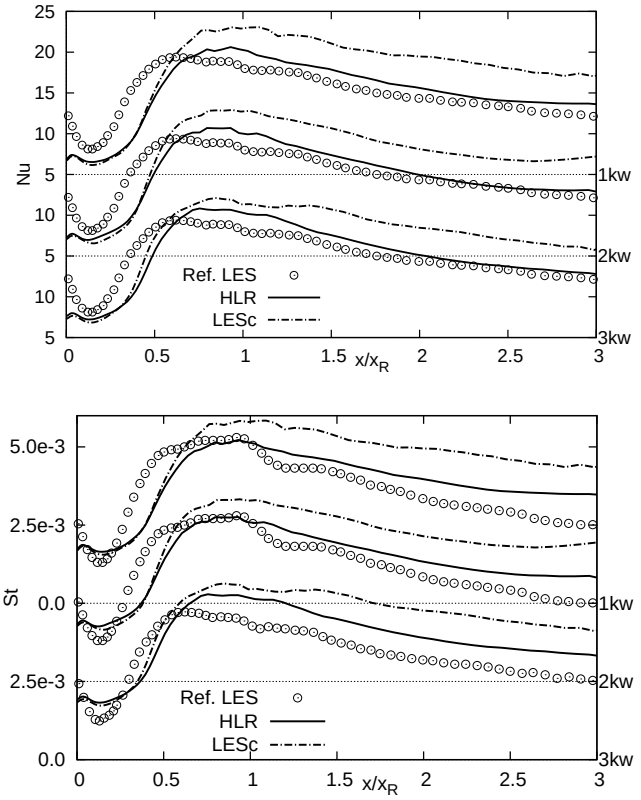

FIGURE 23. Nusselt (upper) and Stanton (lower) number variation for all three cases with wall heating - $q_w = 1$, 2 and $3kW/m^2$

Model, *AIAA Journal*, Vol. 20(1), pp. 33-38

[5] Jakirlic, S., and Hanjalic, K., 2002, A new approach to modelling near-wall turbulence energy and stress dissipation. *J. Fluid Mech.*, Vol. 539, pp. 139-166

[6] Jovic, S. and Driver, D., 1995, Reynolds number effects on the skin friction in separated flows behind a backward-facing step, *Experiments in Fluids*, Vol. 18(6), pp. 464-467

[7] Kasagi, N. and Matsunaga, A., 1995, Three-dimensional particle-tracking velocimetry measurements of turbulence statistics and energy budget in a backward facing step flow, *Int. J. Heat and Fluid Flow*, Vol. 16, pp. 477-485

[8] Keating, A., Piomelli, U., Bremhorst, K., and Nesic, S., 2004, Large-eddy simulation of heat transfer downstream of a backward-facing step. *Journal of Turbulence*, Vol. 5, pp. 1-27

[9] Klein, M., Janicka, J. And Sadiki, A., 2003, A digital filter based generation of inflow data for spatially developing direct numerical or large-eddy simulations. *J. Comp. Physics*, Vol. 186, pp. 652-665

[10] Le, H., Moin, P. and Kim, J., 1997, Direct Numerical Simulation of Turbulent Flow over a Backward-Facing Step, *J. Fluid Mech.*, Vol. 330, pp. 349-374

[11] Mason, P.J., and Callen, N.S., 1986, On the magnitude of the subgrid-scale eddy coefficient in large-eddy simulation of turbulent channel flow. *J. Fluid Mech.*, Vol. **162**, pp. 439-462

[12] Nikitin, N.V, Nicoud F. Wasistho B.-Squires K.D., Spalart,

P.R., 2000, An Approach to Wall Modelling in Large-Eddy Simulations. *Phys. Fluids*, Vol. 12(7), pp. 1629-1632

[13] Piomelli, U., Balaras, E., Pasinato, H, Squires, K.D. and Spalart, P.R., 2003, The inner-outer layer interface in largeeddy simulations with wall-layer models. *Int. J. Heat and Fluid Flow*, Vol. 24(4), pp. 538-550.

[14] Pope, S., 2000, Turbulent flows, Cambridge Univ. Press

[15] Saric, S., Jakirlic, S. and Tropea, C., 2005, A periodically perturbed backward-facing step flow by means of LES, DES and T-RANS: an example of flow separation control, *ASME J. of Fluids Engineering*, Vol. 127, pp. 879-887

[16] Temmerman, L., Hadziabdic, M., Leschziner, M.A., and Hanjalic, K.. 2005, A hybrid two-layer URANS-LES approach for large eddy simulation at high Reynolds numbers. *Int. J. Heat and Fluid Flow*, Vol. **26**, pp. 173-190

[17] Vogel, J.C., and Eaton, J.K., 1985, Combined heat transfer and fluid dynamics measurements downstream of a backward-facing step. *ASME Journal of Heat Transfer*, Vol. 107, pp. 922-929